JOURNAL OF APPLIED ELECTROCHEMISTRY 19 (1989) 485–494

Aluminium dissolution in the $NaF-AlF_3-Al_2O_3$ system: effects of alumina, temperature, gas bubbling and dissolved metal

E. SUM, M. SKYLLAS-KAZACOS

School of Chemical Engineering and Industrial Chemistry, University of New South Wales, PO Box 1, Kensington, NSW 2033, Australia

Received 6 February 1989

Current reversal chronopotentiometry, with and without a delay time between the forward and reverse current pulses, was employed to evaluate the effects of temperature, alumina content, gas bubbling (argon and carbon dioxide) and dissolved metal on the rate of aluminium dissolution in $NaF-AlF_3-Al_2O_3$ molten bath. The working electrode was a tungsten wire electrode and the temperature range studied was 824–1040° C. The effect of the alumina content was determined in melts with CR = 1.45 and CR = 4.3 at 1029 ± 3° C (CR = mol NaF/mol AlF_3). The experiments involving gas bubbling and dissolved metal were carried out in melts similar to industrial compositions, i.e. CR = 2.4, 4.8 wt. % Al_2O_3 at 980° C. In general, the dissolution rate of aluminium increased with increasing temperature, decreased slightly with increasing alumina content in acidic melts (CR < 3) but changed little in basic melts (CR > 3), increased with bubbling and decreased in the presence of dissolved metal. The rate of Al dissolution is thus mass transport controlled.

1. Introduction

There have been numerous studies on aluminium solubility in molten cryolite [1, 2, 3]. Although the data do conflict as a result of variations in experimental procedures, the general trends are usually consistent [1, 2]. Saturation solubility of Al in cryolite has been shown to be affected by temperature and cryolite ratio (CR = molar ratio of NaF/AlF_3 in the bath), however, the effect of alumina is not clear [2]. In contrast, there has been little published on the rate of aluminium dissolution in cryolite systems. The influence of the main parameters of temperature and bath composition on the rate of Al dissolution is important in operation and design of Hall-Heroult cells, most cells being optimized for high current efficiency and/or low energy consumption.

A brief review on published studies concerning the rate of aluminium dissolution in molten cryolite was covered in our earlier paper [4] in which we reported the effect of cryolite ratio on the rate of aluminium dissolution in an unstirred cryolite melt with 4 wt. % Al_2O_3 at 1031° C. The aims of this investigation are to examine the effects of temperature, alumina content, gas bubbling and dissolved metal on the rate of aluminium dissolution.

2. Experimental

The required quantities of synthetic cryolite, alumina and aluminium fluoride (all supplied by Comalco Ltd., Bell Bay, Tasmania, Australia) or sodium fluoride (Laboratory grade, Ajax Chemicals, Sydney, Australia) were pre-mixed to ensure homogeneity on melting, and introduced into a carbon crucible (AGSX or ATJ grade, Carbon Brush Manufacturing Pty. Ltd., Sydney, Australia) with dimensions 45 mm I.D. × 52 mm O.D. × 140 mm inside × 150 mm outside which was fitted with a carbon lid. The crucible and its contents were placed in the isothermal zone of a vertical Kanthal resistance furnace and heated slowly (150–200° C h^{-1}) under an inert atmosphere of dry argon.

The working electrode was a 1 mm diameter tungsten wire electrode (Alfa Products, Danvers, MA 01923, USA) which was immersed 15 mm (unless otherwise stated) into the electrolyte, giving an electrode area of 0.48 cm^2. The depth of immersion could be accurately controlled because the mass of electrolyte was calculated such that its liquid volume would fill the crucible to a depth of 30 mm. The surface of the electrolyte could also be detected using a voltmeter when lowering the tungsten electrode. A similar tungsten wire electrode was used as a quasi-reference electrode and the carbon crucible served as the counter electrode.

The melt temperature was measured with a chromel-alumel thermocouple (Pyrosales, Sydney, Australia). For each set of experiments (one melt composition), the temperature varied only by ± 1° C. A new melt was prepared for each experiment to minimize changes in bath composition, particularly CR, due to evaporation.

In the gas bubbling experiments, the gas was passed

0021-891X/89 $03.00 + .12

into the melt through a recrystallized alumina tube (Pyrosales, Sydney, Australia) with dimensions 4 mm O.D. × 2 mm I.D. A recrystallized alumina tube, instead of a metal tube, was chosen to avoid contamination of the melt by metal ions. During bubbling, the tube was lowered until it touched the bottom of the crucible and then lifted approximately 5 mm from the bottom. The gas, either carbon dioxide (Food Grade, CIG, Sydney, Australia) or argon (ultra-high purity, CIG), was bubbled through the melt only during the delay time between the forward and reverse current pulses in chronopotentiometry. This was done to ensure that the area of the tungsten electrode (determined by the depth of immersion) was the same during the deposition and stripping stages, as well as to ensure that the deposition conditions were the same for all the experiments. The recrystallized alumina tube was kept 10–20 mm above the surface of the melt with gas flowing continuously in between runs so that the tube would not become blocked and to minimize immersion time in the melt. The gas flow rate was varied between 20 and 115 mL min^{-1}.

A large excess of aluminium metal was used in the experiments involving cryolite melts saturated with dissolved metal. A disc of aluminium (Comalco Ltd.), measuring approximately 44 mm dia. × 10 mm thick and weighing 36.9 g, was placed at the bottom of the carbon crucible and then the cryolite-alumina powder mixture was poured on top of it. The mass of Al was calculated to form a layer of about 10 mm thick, when molten, if the metal were flat. In reality, the metal surface is dome-shaped because aluminium does not wet carbon and this was verified at the end of the experiment. When the furnace reached its set temperature, the molten Al and cryolite melt were allowed to stand for 2 hours to ensure that the melt was saturated in dissolved metal.

The conditions for the gas bubbling and dissolved metal experiments were CR = 2.4, 4.8 wt % Al_2O_3 and 980° C; these were chosen as being average industrial operating conditions [1]. The effects of temperature and alumina were studied in acidic (CR < 3) and basic (CR > 3) melts.

The melt was studied using cyclic voltammetry (CV) and current reversal chronopotentiometry (CRC) with and without a delay time (zero current) introduced between the forward and reverse current pulses. An EG & G PARC Model 175 Universal Programmer and PAR Model 173 Potentiostat/Galvanostat were employed and the resulting voltammogram (I–E curve) or chronopotentiogram (E–t curve) was recorded on a Riken-Denshi Model D-8DG X–Y recorder.

3. Results and discussion

3.1. *Temperature*

The melt compositions employed were CR = 6.5, 2.3 wt. % Al_2O_3 (liquidus temperature ≈ 881° C [2]) for the basic melt, and CR = 1.50, 7.6 wt. % Al_2O_3 (liquidus temperature ≈ 822° C [2]) for the acidic melt. These compositions were chosen to achieve a wide temperature range and to ensure that one dissolution reaction was greatly predominant over the other under the conditions of extreme acidity or basicity.

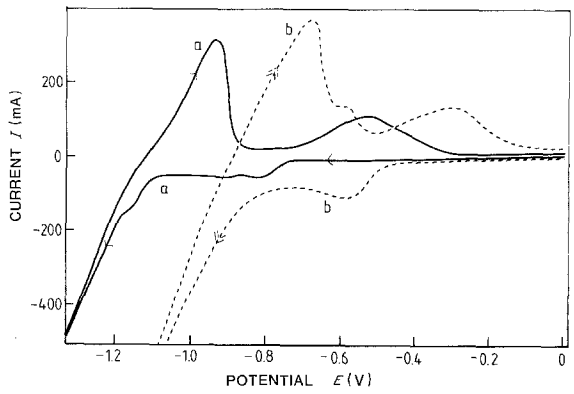

Fig. 1. Cyclic voltammogram of cryolite melt with CR = 1.5, 7.6 wt. % Al_2O_3 at a sweep rate of 100 mV s^{-1}. (a) 918° C; (b) 1040° C.

Two cyclic voltammograms, at temperatures of 918 and 1040° C, are shown in Fig. 1. The general shape of both curves is similar, however, the current is larger at the higher temperature (Fig. 1b) as expected. The additional anodic peak at −0.6 V in Fig. 1b is probably reoxidation of dissolved metal. (cf. chronopotentiogram, Fig. 20).

The multiple cathodic prewave representing alloy or intermetallic compound formation [5] at 918° C merge to become one wave at 1040° C. Similar behaviour is observed as the sweep rate is increased to 500 mV s^{-1} at a given temperature.

The cathodic prewave(s) was studied in greater detail in acidic and basic melts by chronopotentiometry [5]. The number of electrons transferred was calculated to be three, confirming that the reaction involves Al deposition with alloy or intermetallic compound formation.

Current reversal chronopotentiograms obtained at 918° C and 1040° C are shown in Fig. 2. At the higher temperature (Fig. 2b), the potential rises more gradually and the extent of alloy/intermetallic compound formation is greater. There are only two (observable) reverse transitions at the lower temperature (Fig. 2a): the stripping of Al metal, τ_{r2}, and reoxidation of Al–W alloy/intermetallic compound, τ_{r1}. An inflection in τ_{r1} is observed at Q in Fig. 2b, suggesting that more than one kind of alloy is present. In the presence of dissolved metal, additional transitions are observed between τ_{r2} and τ_{r1} (Fig. 20). An inspection of the Al–W phase diagram shows the presence of a solid solution of Al in W (97.4 wt. % W) at approximately 1050° C [6]. Hence, inflection point Q may indicate the presence of this new phase.

The transition times, τ_{r2} and τ_{r1}, represent the amount of Al remaining on the electrode after current reversal. If there were no chemical attack of deposited Al, the sum of τ_{r2} and τ_{r1} should equal t_f for the same forward and reverse current. The transition time ratio, $R = \tau_r/t_f$ where $\tau_r = \tau_{r2} + \tau_{r1}$, is less than 1 in

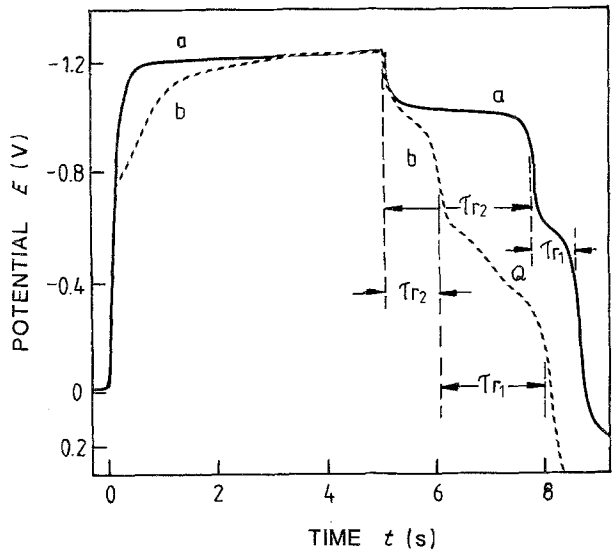

Fig. 2. Chronopotentiograms with current reversal of cryolite melt with CR = 1.5, 7.6 wt. % Al_2O_3. Forward and reverse currents are equal. I = 200 mA and t_f = 5 s. (a) 918° C; (b) 1040° C. For ease of comparison, line (b) is shifted −0.22 V.

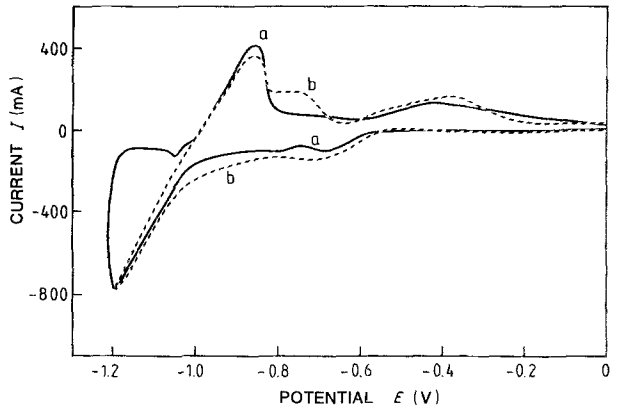

Fig. 4. Cyclic voltammogram of cryolite melt with CR = 6.5, 2.3 wt. % alumina at a sweep rate of 100 mV s^{-1} and reversal potential at −1.2 V. (a) 902° C (b) 965° C.

these experiments, showing that following the charge transfer reaction, some Al is lost in the electrolyte.

By introducing a delay time, t_d, at zero current between the cathodic and anodic current pulses, the rate of Al dissolution at open circuit potential can be obtained. Figure 3 shows that a plot of R vs t_d is a straight line. The rate of Al dissolution r_d, can be calculated from [4]:

$$r_d = b\frac{Q_f}{AnF} \text{ mol cm}^{-2}\text{ s}^{-1} \quad (1)$$

where b = slope of R vs t_d plot (s^{-1})
$Q_f = It_f$ = cathodic charge (C)
A = electrode area (cm^2)
n = number of electrons
F = Faraday constant (C mol^{-1})

Similar voltammetric and chronopotentiometric results were also obtained in a basic melt. Figure 4 shows that the general shapes of the cyclic voltammograms resemble those found in an acidic melt. However, the cathodic current increases more rapidly due to sodium codeposition superimposed on aluminium deposition. In addition, as a result of lower current efficiency with respect to Al deposition and the higher rate of Al dissolution [4], the stripping of Al appears as a smaller peak. At 902° C, a separate peak for Al deposition, distinct from sodium reduction, is observed in the cyclic voltammogram of Fig. 4a. Chronopotentiograms also exhibit a separate transition for Al deposition [5]. Similar voltammetric peak and chronopotentiometric transition were observed in an acidic melt below 850° C [5].

The Al dissolution rates are shown in Fig. 5 as a function of temperature. The rate of Al dissolution decreases with temperature and then levels off between 820 and 900° C. The corresponding Arrhenius plot is shown in Fig. 6, the slope of which yields an activation energy E_a = 69 kJ mol^{-1} for the reaction of Al with Al(III) as represented by equation (2).

$$2Al + Al(III) \rightleftharpoons 3Al(I) \quad (2)$$

At temperatures close to the liquidus temperature of approximately 882° C, the measured rates of Al dissolution are greater than that at 844° C. This anomaly could be attributed to a change in the electrolyte composition near the surface of the electrode as a result of precipitation of solid Na_3AlF_6. The liquidus curve is extremely steep in the vicinity of

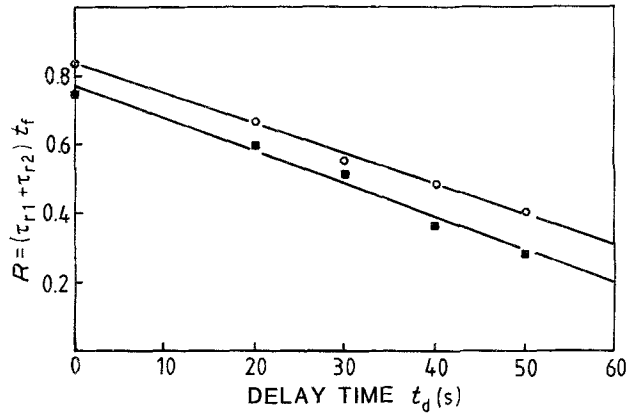

Fig. 3. Variation of transition time ratio, R, with delay time for CR = 1.5, 7.6 wt. % alumina at 844° C. $\tau_r = \tau_{r2} + \tau_{r1}$ (see text). (a) I = 200 mA, t_f = 10 s; (b) I = 400 mA, t_f = 5 s. ■, 200 mA, 10 s; ○, 400 mA, 5 s.

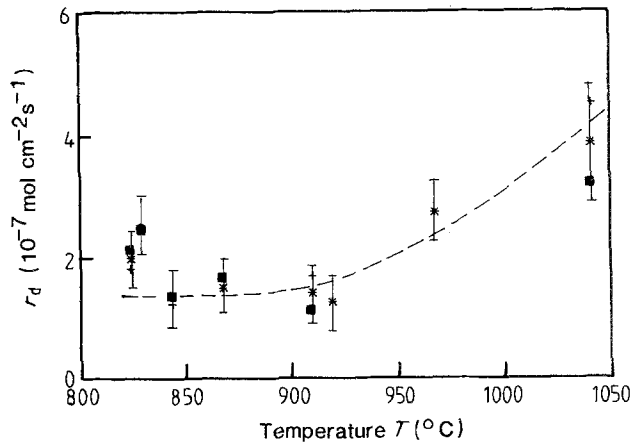

Fig. 5. The effect of temperature on the rate of Al dissolution in an acidic melt with CR = 1.50 and 7.6 wt. % Al_2O_3. ■, 0.4 A cm^{-2}; +, 0.8 A cm^{-2}; (*), means values.

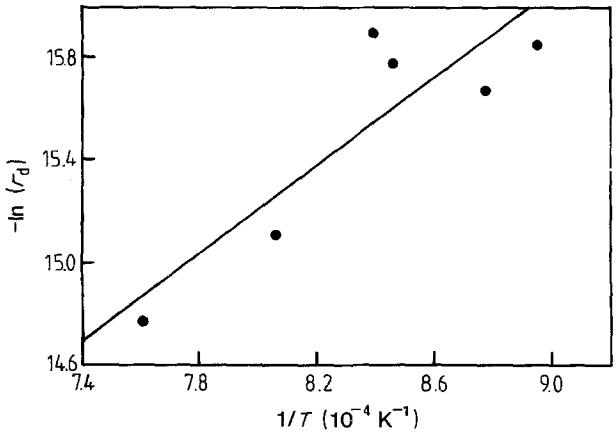

Fig. 6. Arrhenius plot for cryolite melt with CR = 1.50 and 7.6 wt. % Al_2O_3.

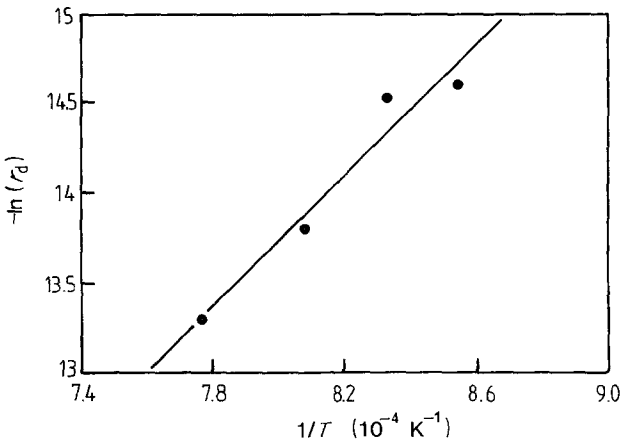

Fig. 8. Arrhenius plot for cryolite melt with CR = 6.5 and 2.3 wt. % Al_2O_3.

40 mol % AlF_3 (CR = 1.5), as revealed by the NaF–AlF_3 phase diagram [2]. A reduction of only 2–3 mol % AlF_3 at 824° C would cause Na_3AlF_6 to precipitate. The cryolite ratio near the cathode increases during metal deposition due to accumulation of Na^+ (the main current carrier) [8]. The shift towards higher CR due to Na^+ build-up and Na_3AlF_6 precipitation near the electrode surface therefore causes the observed rate of aluminium dissolution to be higher than expected. There was no blockage of the electrode surface by an insulating layer of frozen electrolyte which would reveal itself as a huge increase in resistance. Due to these changes in electrolyte composition, the r_d data at 824 and 830° C were not included in the calculation of the activation energy for reaction (2).

In the basic melt, the variation of r_d with temperature is much greater than in the acidic melt although the general trend is similar (Fig. 7). The corresponding Arrhenius plot is shown in Fig. 8 and the activation energy for the reaction between Al and Na^+ (equation 3) was calculated to be E_a = 151 kJ mol^{-1}.

$$Al + 3Na^+ \rightleftharpoons Al(III) + 3Na(0) \qquad (3)$$

Metal solubility in general increases monotonically with temperature [2, 7] but the change is not very big, e.g. for a temperature rise of about 100° C, the solubility increased by approximately 1.6 times [7].

Bersimenko and Vetyukov [9] measured the aluminium loss rate as a function of temperature in a cryolite melt with CR = 2.8 and 5 wt. % Al_2O_3 in the temperature range of 960 to 1025° C. The increase in Al loss rate with temperature was attributed to increased Al solubility and decreased melt viscosity. They calculated the effective activation energy for two different additions of 3 mol % MgF_2 + LiF and 6 mol % MgF_2 to be 52.8 and 35.3 kcal mol^{-1} (221 and 148 kJ mol^{-1}), respectively. LiF was added to compensate for the drop in conductivity and increase in melt viscosity caused by the addition of MgF_2.

The low values of activation energy (69 and 151 kJ mol^{-1}) tend to indicate a diffusion process, as suggested by Bersimenko and Vetyukov [9]. The E_a values obtained in this study are lower than those in reference [9] because of differences in interfacial tension between metal and melt, and viscosity. In general, viscosity isotherms exhibit a maximum in the vicinity of Cr = 3 and fall away for CR < 3 and CR > 3 [2].

3.2. *Alumina concentration*

The rate of Al dissolution was determined at constant temperature (1029 ± 3° C) in both acidic and basic

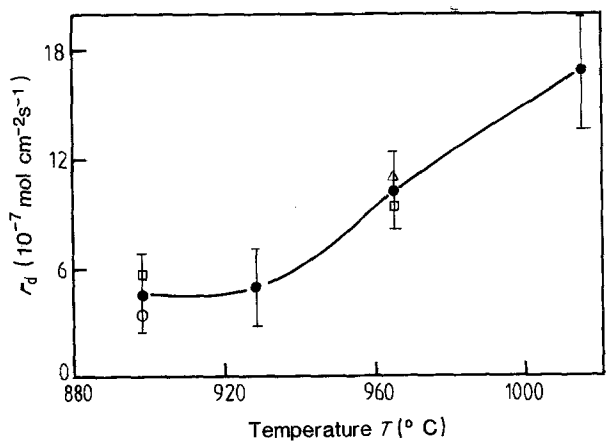

Fig. 7. The effect of temperature on the rate of Al dissolution in a basic melt with CR = 6.5 and 2.3 wt. % Al_2O_3. ●, mean values; ○, 0.6 A cm^{-2}; +, 0.8 A cm^{-2}; □, 1.0 A cm^{-2}; △, 1.2 A cm^{-2}.

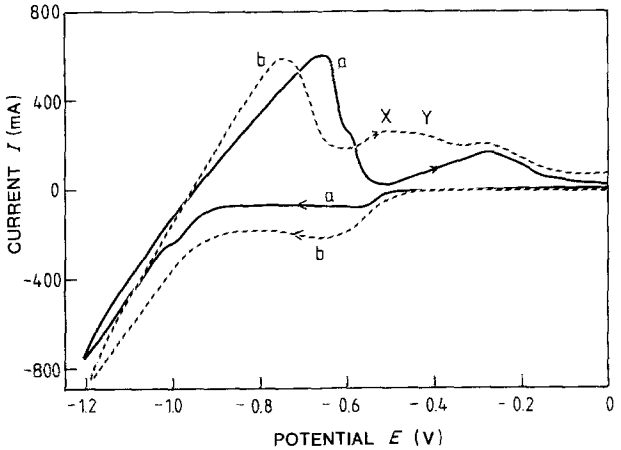

Fig. 9. Cyclic voltammogram of an acidic melt with CR = 1.45 and 1.95 wt. % alumina at 1026° C. W wire electrode area = 0.48 cm^2 (a) 50 mV s^{-1}; (b) 500 mV s^{-1}.

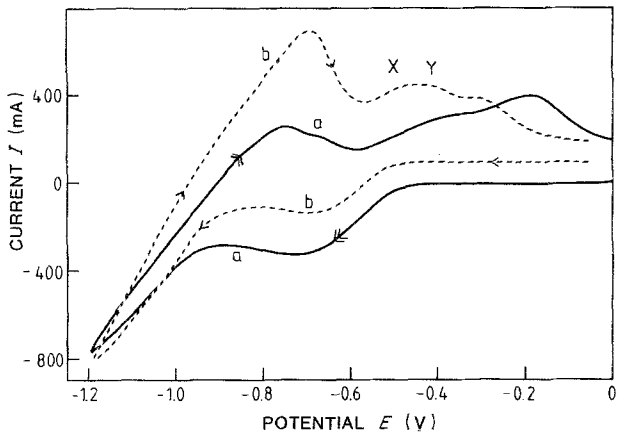

Fig. 10. Cyclic voltammogram of an acidic melt with CR = 1.45 at 1030° C and v = 500 mV s^{-1}. W wire electrode area = 0.48 cm^2. (a) 6.1 wt. % Al_2O_3 (b) 9.75 wt. % Al_2O_3.

melts by the method of CRC with delay. The electrolyte composition were CR = 1.45 (acidic) and CR = 4.3 (basic).

The effect of alumina on the overall cyclic voltammogram in an acidic melt can be seen in Figs 9 and 10. The cathodic prewave increases in size as the alumina content is increased from 1.95 to 6.1 wt. % but it decreases in size as the alumina content is increased further to 9.75 wt. %. This prewave has been shown to be diffusion-controlled with a diffusion coefficient of the order of 10^{-9} cm^2 s^{-1} which is too low to be electrolyte diffusion [5]. The variation of the height of the prewave with alumina content may thus reflect a variation in the surface layer thickness due to different film dissolution rate with changing melt composition.

Additional peaks, X and Y, appear during the anodic scan at the higher sweep rate of 500 mV s^{-1} in Figs 9 and 10. These anodic peaks are ascribed to the oxidation of dissolved metal species, possibly Al(I) and Na(0) [2, 3], which were formed during dissolution of deposited Al. At lower scan rates, e.g. Fig. 9a, these dissolved metal species have diffused away and are not detected on the anodic scan.

Cyclic voltammograms obtained in a basic melt (CR = 4.3) are shown in Fig. 11. Peaks X and Y in Figs 9 and 10 for the acidic melt are no longer obvious. Like the acidic melt, the effect of alumina on the Al

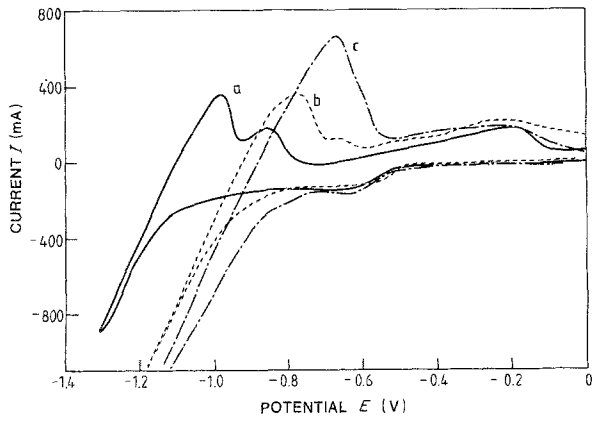

Fig. 11. Cyclic voltammogram of a basic melt with CR = 4.3 and at 1027° C and v = 100 mV s^{-1}. Reversal potential at −1.3 V. W wire electrode area = 0.48 cm^2. (a) 0 wt. + Al_2O_3; (b) 2 wt. % Al_2O_3; (c) 7 wt. % Al_2O_3.

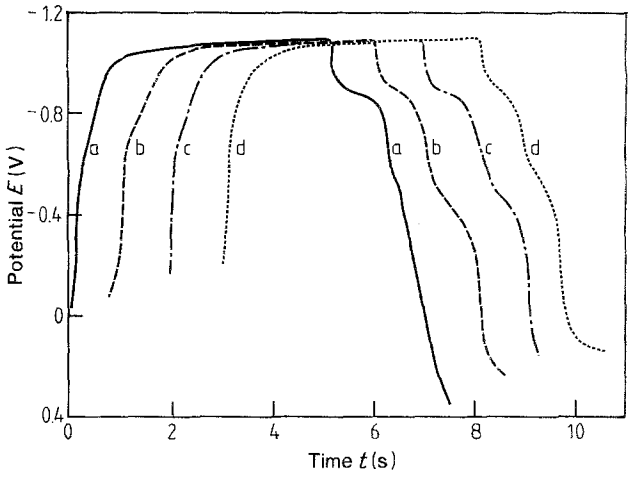

Fig. 12. Current reversal chronopotentiograms of a basic melt with CR = 4.3 at 1027 ± 1° C for various alumina contents. (a) 0 wt. %; (b) 2 wt. %; (c) 4 wt. %; (d) 7 wt. %.

stripping peak in a basic melt is indirect, i.e. alumina influences the chemical equilibria involving Al(III) complexes and thus affects the concentration of the attacking species during the dissolution process. However, the chronopotentiograms do not differ much for various alumina concentrations (Fig. 12), unlike those for acidic melts. Current reversal chronopotentiograms obtained in an acidic melt (Fig. 13) show the same trend for the stripping of Al as in cyclic voltammetry. The rate of Al dissolution for different alumina concentrations are plotted in Figs 14 and 15. In both acidic and basic melts, there is no apparent, or little, variation of the rate of Al dissolution with alumina concentration. If a dependence existed, the spread of the data allows one to draw a straight line of negative slope or a curve with a maximum between 4–6 wt. % Al_2O_3 for CR = 1.45 in Fig. 14, and a similar curve for CR = 4.3 in Fig. 15.

The effect of alumina on the rate of Al dissolution is probably physical rather than chemical, hence the difficulty in determining such effects with great accuracy.

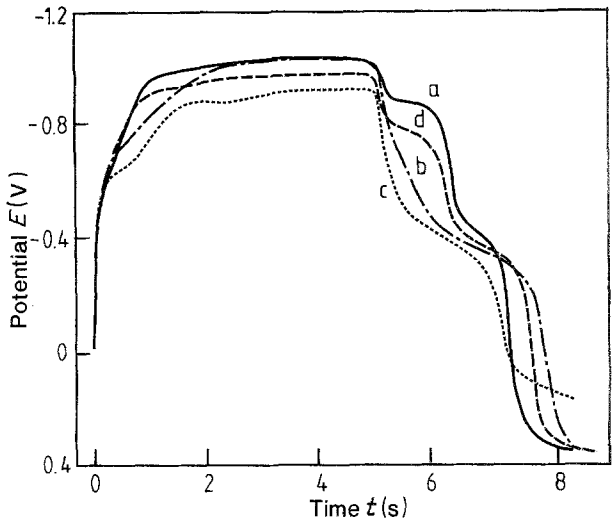

Fig. 13. Current reversal chronopotentiograms of an acidic melt with CR = 1.45 at 1029 ± 3° C for various alumina contents. (a) 1.95 wt. %; (b) 4 wt. %; (c) 6.1 wt. %; (d) 9.76 wt. %.

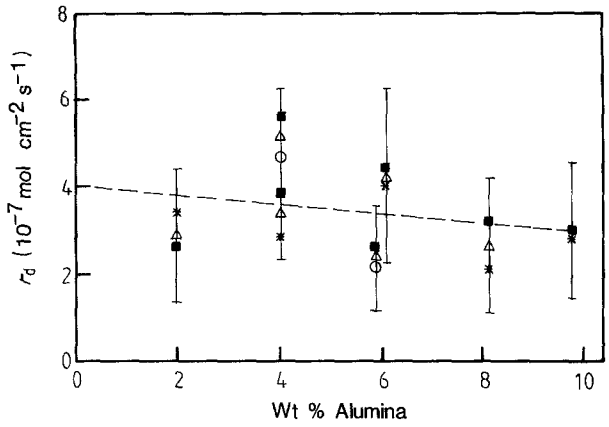

Fig. 14. The effect of alumina concentration on the rate of Al dissolution in the acidic melt with CR = 1.45, at 1029 ± 3°C. *, 0.4 A cm^{-2}; ○, 0.6 A cm^{-2}; ■, 0.8 A cm^{-2}; △, mean values.

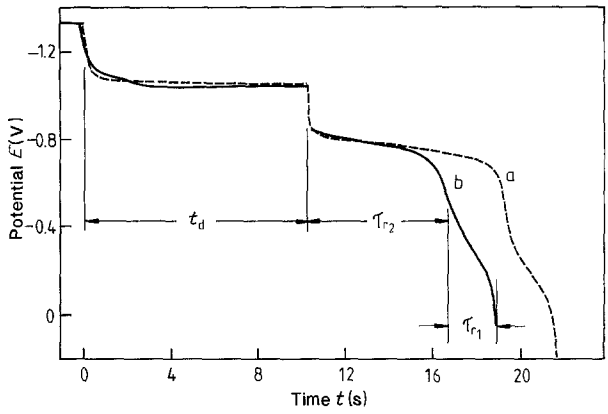

Fig. 16. Bubbling with carbon dioxide and argon during delay time before current reversal in chronopotentiometry. I = 400 mA, t_f = 20 s and t_d = 10 s. (a) 22 mL Ar min^{-1} (979°C); (b) 27 mL CO_2 min^{-1} (984°C).

The addition of alumina changes the liquidus line in phase diagrams, hence changing the degree of superheat [1, 2] for a given melt temperature. This degree of superheat is a determining factor for aluminium loss [2].

Increasing the alumina concentration increases the viscosity of the melt [1, 2, 3]. Increase in viscosity would hinder the diffusion of the attacking species from the bulk electrolyte and the diffusion of products away from the reaction zone. Therefore, the rate of Al dissolution would be expected to decrease as alumina concentration increases, but the change would be small.

3.3. *Gas bubbling*

The following three sets of experiments were carried out in a melt with CR = 2.4 and 4.8 wt. % Al_2O_3 using the technique of current reversal chronopotentiometry with a delay time between the forward and reverse current pulses.

(1) No bubbling (979 ± 2°C).

(2) Bubbling with U.H.P. argon during delay (979 ± 1°C).

(3) Bubbling with food-grade carbon dioxide during delay (984 ± 2°C).

The average temperature over all the experiments was 981 ± 3°C.

At zero delay time, i.e. no bubbling through the melt, the current reversal chronopotentiograms were the same, regardless of whether argon or CO_2 was flowing above the surface of the electrolyte. Figure 16 shows the variation in electrode potential during a 10-second delay and anodic pulse, following the deposition of Al at I = 400 mA and t_f = 20 s. For all three cases at t_d = 0, τ_{r2} = 13.1 ± 0.3 s and τ_{r1} = 1.3 ± 0.2 s. For similar gas flow rates, the value of τ_{r2} is smaller for CO_2, showing that less aluminium remains on the electrode after bubbling CO_2 compared to argon (Fig. 16). Noise signals superimposed on the potential transient during t_d are usually observed as a result of gas flowing past the electrode surface. These noise signals are not apparent in Fig. 16 because of low flow rates.

The transition time ratio, $R = \tau_r/t_f$ for each of the three cases are plotted versus t_d in Figs 17, 18 and 19, where $\tau_r = \tau_{r2} + \tau_{r1}$. A linear relationship is observed for the two cases of no gas flowing (Fig. 17) and for argon bubbling (Fig. 18). The plot for the CO_2 bubbling experiment however, shows a steep curve initially, becoming linear for $t_d > 5$ s (Fig. 19).

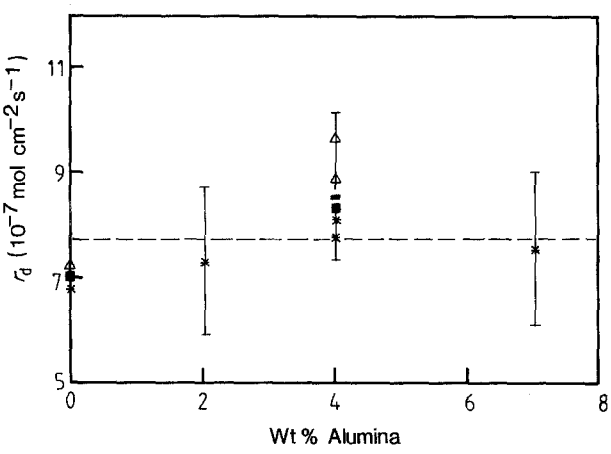

Fig. 15. The effect of alumina concentration on the rate of Al dissolution in a basic melt with CR = 4.32 at 1027 ± 1°C. *, 0.8 A cm^{-2}; △, 1.0 A cm^{-2}; ■, mean values.

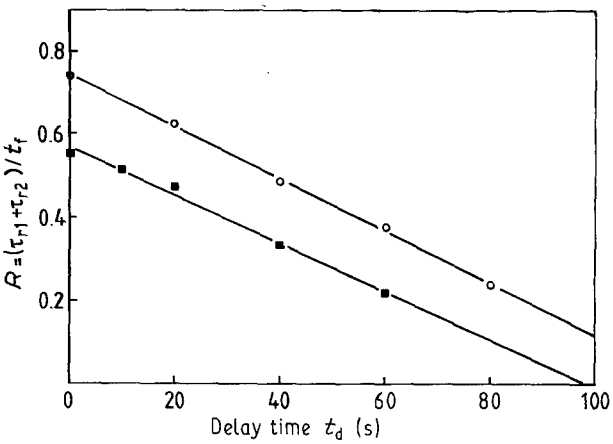

Fig. 17. Variation of R = τ_r/t_f with delay time without any gas bubbling. $\tau_r = \tau_{r2} + \tau_{r1}$ and Q_f = 8°C. CR = 2.4, 4.8 wt. % alumina at 979°C. (a) I = 200 mA, t_f = 40 s; (b) I = 400 mA, t_f = 20 s. ■, 200 mA, 40 s; ○, 400 mA, 20 s.

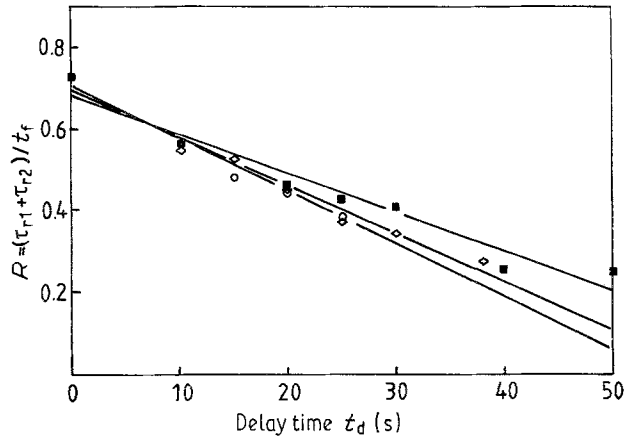

Fig. 18. Variation of $R = \tau_r/t_f$ with delay time with argon gas flowing. $\tau_r = \tau_{r2} + \tau_{r1}$ and $Q_f = 8\,C$ ($I = 400\,mA$, $t_f = 20\,s$). CR = 2.4, 4.8 wt. % alumina at 979° C. (a) ■, 22 mL min^{-1}; (b) ◇, 45 mL min^{-1}; (c) 85 mL min^{-1}.

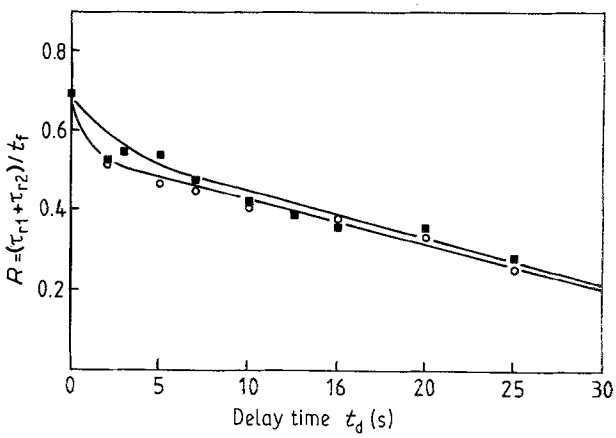

Fig. 19. Variation of $R = \tau_r/t_f$ with delay time with CO_2 gas flowing. $\tau_r = \tau_{r2} + \tau_{r1}$ and $Q_f = 8\,C$ ($I = 400\,mA$, $t_f = 20\,s$). CR = 2.4, 4.8 wt. % alumina at 984° C. (a) ■, 27 mL min^{-1}; (b) ○, 114 mL min^{-1}.

The steep initial portion may also exist for argon gas bubbling but it is not observed because there is no data for $0 < t_d < 10$ s. From Fig. 18, it seems that the initial curvature, if it existed, would not be as obvious as for CO_2 bubbling. The rates of Al dissolution for CO_2 bubbling in Table 1 are calculated from the linear slopes in Fig. 19.

The results in Table 1 show that the rate of Al dissolution is controlled by mass transfer of attacking species. There is hardly any difference between argon and CO_2 bubbling for similar flow rates. Hence, the direct oxidation of dissolved metal or Al on the electrode by CO_2 is minimal under steady-state conditions. Oblakowski and Orman [10] also reported that the rate of Al loss depends on the degree of mixing and not on the oxidizing ability of the gas bubbling through the melt (CO_2, air or argon). No direct reaction between Al and CO_2 was observed and they obtained an Al loss rate of 0.0507 g cm^{-2} h^{-1} (5.22×10^{-7} mol cm^{-2} s^{-1}) for a flow rate of 4.01 h^{-1} (67 ml min^{-1}). Our results agree very well with those of Orman and Oblakowski [10].

Initially when $t_d < 5$ s, there is a chemical contribution from CO_2 towards Al loss as indicated in Fig. 19 and also in Fig. 17. The reaction may be represented by

$$2Al_{(diss)} + 3CO_2 \rightleftharpoons Al_2O_{3(diss)} + 3CO \qquad (4)$$

where $Al_{(diss)}$ could be Al or Na species in solution [1, 2, 3]. At $t_d = 0$, there is an accumulation of dissolved metal near the electrode as a result of dissolution occurring during t_f. Hence, the rate of reaction (4) is fast initially at short t_d and the accumulated dissolved metal near the electrode is removed quickly by the combined action of chemical attack and physical dissipation by CO_2. Therefore, the aluminium deposited on the electrode dissolves quicker initially when bubbling with CO_2 compared to argon.

3.4. *Chronopotentiometry in cryolite melts containing molten aluminium*

In the presence of a huge excess of molten aluminium, the tungsten wire electrode behaves like an aluminium electrode due to the presence of dissolved metal in the melt [2]. This is observed in our studies – the equilibrium potential is shifted cathodically by about 0.9 V in the presence of dissolved metal such that initial

Table 1. Rate of Al dissolution and gas bubbling. CR = 2.4, 4.8 wt. % Al_2O_3 at 981 ± 3° C. Current reversal chronopotentiometry with delay at a tungsten wire electrode, $Q_f = 8°\,C$

Gas	*Flow rate* $ml\,min^{-1}$	*i* $A\,cm^{-2}$	$r/10^{-7}\,mol\,cm^{-2}\,s^{-1}$ $R = \frac{\tau_{r2} + \tau_{r1}}{t_f}$	*Reference*
None	0	0.36	2.89	This work
		0.73	3.14	
Argon	22	0.83	5.56	
	45	0.83	6.82	
	85	0.83	7.44	
CO_2	27	0.83	5.48	
	114	0.83	5.67	
Air	67	–	5.22)	[10]
			) CR = 3	
Argon	67	–	5.22) 10 wt. % Al_2O_3	
			) 1000° C	
CO_2	67	–	5.22)	

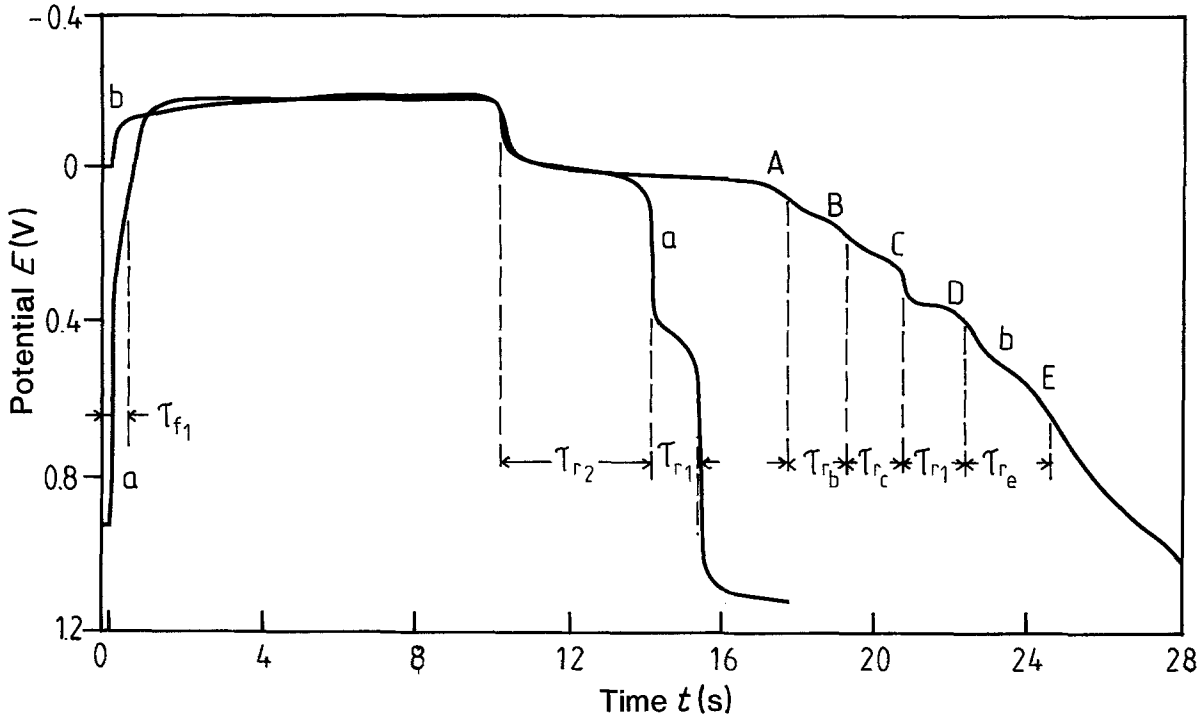

Fig. 20. Effect of dissolved metal on the chronopotentiogram of a melt with CR = 2.4, 4.8 wt. % alumina at 978° C. I = 200 mA and t_f = 10 s. (a) No Al present, (b) Al saturated.

deposition of Al to form Al–W alloy/intermetallic compound (τ_{f1}) no longer occurs and the applied potential for Al deposition is reduced to 0.1 V (including IR), as shown in Fig. 20.

The oxidation of dissolved metal is represented by two transitions between τ_{r2} and τ_{r1}, viz. τ_{rb} and τ_{rc} (Figure 20), which are very close together, barely distinguishable, especially at higher currents. When no Al is present, the potential jumps straight to oxidation of W metal when anodic current is applied. It is not known with certainty what the series of waves after τ_{r1}, e.g. τ_{re}, represent. They could be ascribed to oxidation of other species such as dissolved Al_4C_3 which is not present (or is negligible) in the absence of an Al phase

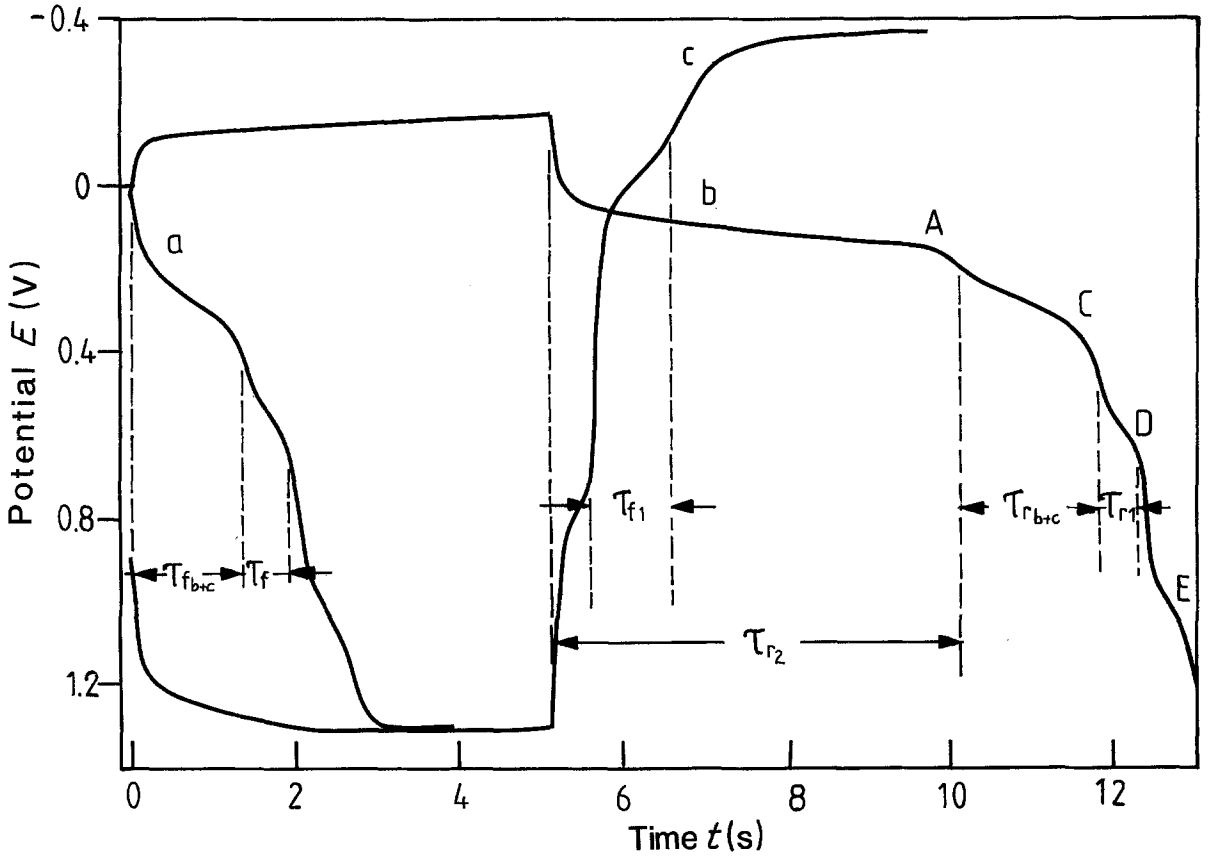

Fig. 21. CR = 2.4, 4.8 wt. % alumina and Al saturated at 978° C. I = 400 mA and t_f = 5 s (in b) (a) anodic chronopotentiometry (Al saturated); (b) cathodic/anodic chronopotentiometry (Al saturated); (c) anodic/cathodic chronopotentiometry (No Al).

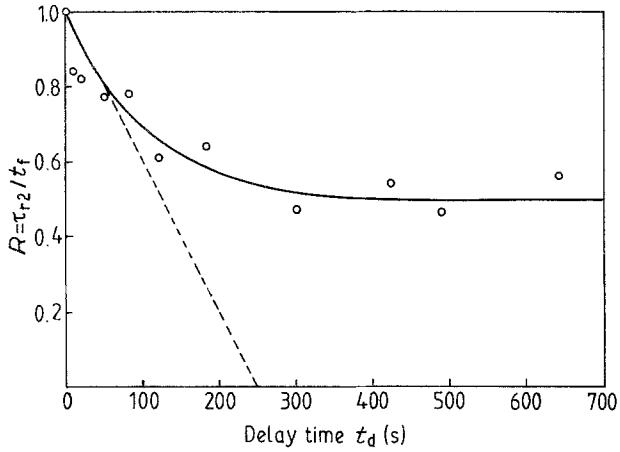

Fig. 22. Variation of $R = \tau_{r2}/t_f$ with delay time for CR = 2.4, 4.8 wt. % alumina, saturated in Al at 978° C. I = 400 mA and t_f = 5 s. ○, 400 mA, 5 s.

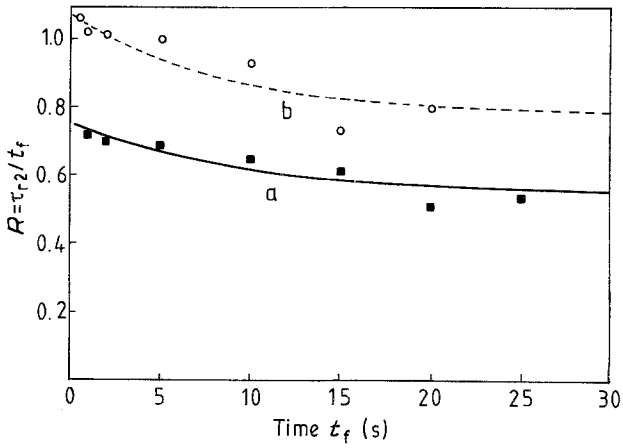

Fig. 23. Variation of $R = \tau_{r2}/t_f$ with t_f in current reversal chronopotentiometry for CR = 2.4, 4.8 wt. % alumina + Al at 978° C. (a) I = 200 mA; (b) I = 400 mA. ■, 200 mA; ○, 400 mA.

in a carbon crucible. Al_4C_3 forms rapidly when aluminium, molten cryolite and carbon are present simultaneously and Al_4C_3 dissolves to form $Al_3FC_8^{3-}$ [11] which can be reoxidized according to

$$Al_3CF_8^{3-} + F^- \rightleftharpoons C_{(s)} + 3AlF_{3(diss)} + 4e^- \qquad (5)$$

The potential for (5) versus an aluminium reference electrode is approximately +0.5.V on a vitreous carbon electrode for I = 2A ($\simeq$ 0.5 A cm^{-2}) at 969° C in a cryolite melt with CR = 2.25 [11]. The series of indistinguishable waves begin at about +0.5 V (Fig. 20b) for I = 200 mA (0.4 A cm^{-2}) at 978° C in a cryolite melt with CR = 2.4, 4.8 wt. % Al_2O_3 in the presence of Al.

It is also clear from Fig. 20 that the rate of Al dissolution is decreased in the presence of dissolved metal since τ_{r2} is larger. τ_{r1} is similar in magnitude in both melts because the surface of the tungsten electrode is already covered with a layer of Al–W alloy/intermetallic compound at t = 0 in the Al saturated melt. This is confirmed in an anodic chronopotentiogram as shown in Fig. 21.

The effect of delay time on the loss of Al is shown in Fig. 22. The slope at any point on the curve is a measure of the rate of Al loss as a consequence of dissolution into the melt (τ_{rb} and τ_{rc}) and the growth of the Al–W alloy (τ_{r1}). The sum of τ_{rb} and τ_{rc} increases with t_d, indicating that dissolution is occurring. τ_{r1} is observed to increase and then remain steady for t_d > 80 s, showing no further growth of the Al–W alloy phase.

If the transition time ratio is calculated as $R = (\tau_{r2} + \tau_{r1} - \tau_{r1}^0)/t_f$ where τ_{r1}^0 is the amount of alloy present at t_d = 0, R is found to be approximately 1 for all t_d. This suggests that no dissolution occurs at all which is contrary to the observed increase in $\tau_{rb} + \tau_{rc}$ with t_d. One possible explanation is the spontaneous deposition of Al from a colloidal suspension of Al in the melt, a quantity which cannot be measured. Under similar conditions but without dissolved metal present, the effect of alloying on the loss of Al was negligible compared to the rate of dissolution (Table 2). Hence, we may take Fig. 22 as a good approximation of the rate of Al dissolution in the presence of a molten Al pad. The initial rate of Al dissolution is 4.98 × 10^{-8} mol cm^{-2} s^{-1} and the rate decreases to zero for t_d > 300 s. This shows that in a melt saturated with dissolved metal, Al dissolution

Table 2. The effect of dissolved metal on the rate of Al loss at a tungsten wire electrode (A = 0.55 cm^2) in a cryolite-alumina melt with CR = 2.4, 4.8 wt. % Al_2O_3 at 978 ± °C

Al saturation	*Method*	*i/A cm^{-2}*	*r_d/10^{-8} mol cm^{-2} s^{-1}*	
			No correction for alloy growth	*Corrected for alloy growth*
No Al present	CRC with delay	0.36	30.5	28.9
		31.7	31.7	31.4
	CRC	0.36	–	38.6
		0.73	55.1	44.3
Some Al present	CRC with delay	0.36	7.00	4.06
		0.73	6.90	4.33
	CRC	0.36	34.4	31.4
Fully saturated	CRC with delay	0.73	4.98 (initial)	–
			0 (steady-state)	–
	CRC	0.73	27.9	13.2

still occurs near the electrode surface because CR is increased as a result of cathodic polarization [10], leading to a greater saturation solubility near the electrode [2, 7].

Results from current reversal chronopotentiometry also show that dissolution occurs at a higher rate during electrolysis. The rate of dissolution calculated from the limiting value of $R = \tau_{r2}/t_f$ [4] in Fig. 23 is 2.79×10^{-7} mol cm^{-2} s^{-1} for $I = 400$ mA.

A summary of the effect of dissolved metal on the rate of Al dissolution/loss is given in Table 2. The presence of dissolved metal reduces the rate of Al dissolution, much more under open circuit conditions than during electrolysis. These results and those on gas bubbling (Section 3.3) support the physical dissolution model proposed by Duruz and Landolt [12], i.e. the dissolution rate of Al is mass transport controlled.

4. Conclusion

The results of this study show that the rate of aluminium dissolution decreases when the temperature is lowered and is only slightly affected by the alumina concentration in the electrolyte. The observed trends follow those for metal solubility [2, 3]. In an industrial situation, the electrolyte is turbulent due to gas bubbles from the carbon anode and the relative velocity between the bath and the liquid aluminium pad is high as a result of magnetic fields. Since our data were obtained in unstirred melts, the data cannot be applied directly to industrial situations, but the observed trends are still valid. The effect of alumina on current efficiency will be greater in industrial cells because the alumina content affects the bubble surface area [3]. This effect on bubbles may be more important than the effect of alumina on metal solubility in the overall mechanism of the back-reaction.

The rate of aluminium dissolution is controlled by mass transport. The rate increases as the flow rate of the gas is increased but it is not dependent on the chemical activity of the gas (argon or CO_2). The presence of dissolved metal reduces the rate of Al dissolution. It is decreased to zero when the melt is fully saturated in dissolved metal. However, during electrolysis, deposited Al continues to dissolve even in a fully saturated melt because the cryolite ratio near the electrode has increased and the solubility of Al near the electrode is greater than in the bulk electrolyte where CR is lower.

The temperature, alumina content, gas bubbling and dissolved metal concentration in the molten bath all affect the rate of dissolution of Al. However, these factors are not independent of each other. Although interaction among the factors has been neglected, the general trends observed in this study are believed to be valid even in industrial cells.

Acknowledgements

The authors wish to thank Comalco Ltd for providing materials and financial support for this project and also for the permission to publish these results. We would also like to thank Professor B. J. Welch (University of Auckland, New Zealand) for his comments on the manuscript.

References

[1] K. Grjotheim and B. J. Welch, *Aluminium Smelter Technology*, Aluminium-Verlag, Düsseldorf (1980).
[2] K. Grjotheim *et al. Aluminium Electrolysis, 2nd Edition*, Aluminium-Verlag, Düsseldorf (1982).
[3] K. Grjotheim and H. Kvande, *Understanding the Hall-Heroult Process for Aluminium Production*, Aluminium-Verlag, Düsseldorf (1986).
[4] E. Sum and M. Skyllas-Kazacos, in press, *J. App. Electrochem.*
[5] E. Sum and M. Skyllas-Kazacos, in press, *Electrochim. Acta.*
[6] M. Hansen and K. Anderko, *Constitution of Binary Alloys, 2nd. edn.*, McGraw Hill, New York (1958).
[7] R. Odegard, A. Sterten and J. Thonstad, *Light Metals* (1987) 389–398.
[8] J. Thonstad and S. Rolseth, *Electrochimica Acta*, **23** (1978) 233–241.
[9] O. P. Bersimenko and M. M. Vetyukov, *Sov. J. Non-Ferrous Met.*, **8** (5) (1967) 71–74.
[10] R. Oblakowski and Z. Orman, *Arch. Hutn.*, **18** (1) (1973) 39–52.
[11] R. Ødegård, Å. Sterten and J. Thonstad, *J. Electrochem. Soc.*, **134** (5) (1987) 1088–1092.
[12] J. J. Duruz and D. Landolt, *Applied Electrochemistry*, **15** (1985) 393–398.